Journal of Neuroscience Methods 182 (2009) 6–16

Contents lists available at ScienceDirect

Journal of Neuroscience Methods

journal homepage: www.elsevier.com/locate/jneumeth

Design and fabrication of a polyimide-based microelectrode array: Application in neural recording and repeatable electrolytic lesion in rat brain

You-Yin Chen[a,*], Hsin-Yi Lai[a], Sheng-Huang Lin[b], Chien-Wen Cho[a], Wen-Hung Chao[c], Chia-Hsin Liao[d,e], Siny Tsang[f], Yi-Fan Chen[g], Si-Yue Lin[g]

[a] Department of Electrical and Control Engineering, National Chiao Tung University, No. 1001, Ta-Hsueh Road, Hsinchu 300, Taiwan, ROC
[b] Department of Neurology, Buddhist Tzu Chi General Hospital, No. 707, Sec. 3, Zhong Yang Road, Hualien 970, Taiwan, ROC
[c] Department of Biomedical Engineering, Yuanpei University, No.306, Yuanpei St., Hsinchu 300, Taiwan, ROC
[d] Department of Research, Buddhist Tzu Chi General Hospital, No. 707, Sec. 3, Zhong Yang Road, Hualien 970, Taiwan, ROC
[e] Institute of Medical Sciences, Tzu Chi University, No.701, Sec 3, Zhong Yang Road, Hualien 970, Taiwan, ROC
[f] College of Criminal Justice, Sam Houston State University, Huntsville, TX 77341-2296, USA
[g] Department of Applied Science, National Hsinchu University of Education, No. 521, Nanda Road, Hsinchu 300, Taiwan, ROC

ARTICLE INFO

Article history:
Received 12 February 2009
Received in revised form 24 April 2009
Accepted 14 May 2009

Keywords:
Microelectrode array
Polyimide
Electroplating
Chronic recording
Electrolytic lesion

ABSTRACT

The design and testing of a new microelectrode array, the NCTU (National Chiao Tung University) probe, was presented. Evaluation results showed it has good biocompatibility, high signal-to-noise ratio (*SNR*: the root mean square of background noise to the average peak-to-peak amplitude of spikes) during chronic neural recordings, and high reusability for electrolytic lesions. The probe was a flexible, polyimide-based microelectrode array with a long shaft (14.9 mm in length) and 16 electrodes (5 μm-thick and 16 μm in radius); its performance in chronic *in vivo* recordings was examined in rodents. To improve the precision of implantation, a metallic, impact-resistant layer was sandwiched between the polyimide layers to strengthen the probe. The three-dimensional (3D) structure of electrodes fabricated by electroplating produced rough textures that increased the effective surface area. The *in vitro* impedance of electrodes on the NCTU probe was $2.4 \pm 0.52\ M\Omega$ at 1 kHz. In addition, post-surgical neural recordings of implanted NCTU probes were conducted for up to 40 days in awake, normally behaving rats. The electrodes on the NCTU probe functioned well and had a high *SNR* (range: 4–5) with reliable *in vivo* impedance (<0.7 MΩ). The electrodes were also robust enough to functionally record events, even after the anodal current (30 μA, 10 s) was repeatedly applied for 60 times. With good biocompatibility, high and stable *SNR* for chronic recording, and high tolerance for electrolytic lesion, the NCTU probe would serve as a useful device in future neuroscience research.

1. Introduction

Implantable microelectrode arrays have advanced the study of brain function by simultaneously recording signals from different groups of neurons, gathering spatiotemporal information regarding complex neural processes (Butovas and Schwarz, 2003; Chen et al., 2004). Rigid silicon-based microelectrode arrays (Csicsvari et al., 2003; Norlin et al., 2002; Shi et al., 2006; Xu et al., 2002) have been fabricated using semiconductor production methods and advanced microelectro-mechanical systems (MEMS). These microelectrode arrays showed desirable features, with precisely defined recording-site configurations, high-density electrode placement capabilities, and potential combinations with on-chip integrated circuitry (Cheung et al., 2007; Vetter et al., 2004).

Nevertheless, micromotion at tissue–electrode contact sites has been a major problem in the application of silicon-based microelectrode arrays for chronic recording. The mismatch between the stiff microelectrode array (silicon or glass substrate) and soft tissue aggravates micromotion, inducing inflammation at the implant site (Biran et al., 2007; Suner et al., 2005). Reactive astrocytes build up, encapsulating the electrode and isolating it from the surrounding neural tissue, which leads to the eventual breakdown of the electrode's recording ability (Biran et al., 2007; Polikov et al., 2005; Schwartz et al., 2006). Microelectrode arrays based on flexible substrates may reduce micromotion and alleviate tissue encapsulation of the implant caused by inflammatory response (Cheung, 2007). Signal stability and quality were maintained for chronic recording. Polymer materials such as polyimide (Cheung et al., 2007; Ludwig et al., 2006), benzocyclobutent (Lee et al., 2004a)

* Corresponding author. Tel.: +886 3 571 2121x54427; fax: +886 3 612 5059.
E-mail address: irradiance@so-net.net.tw (Y.-Y. Chen).

0165-0270/$ – see front matter © 2009 Elsevier B.V. All rights reserved.
doi:10.1016/j.jneumeth.2009.05.010

and parylene (Seymour and Kipke, 2007) have been used in the development of flexible microelectrode arrays. Polyimide showed good biocompatibility and high mechanical flexibility; it was easily manufactured with MEMS technology (Cheung, 2007; Richardson et al., 1993). However, the application of the polyimide substrate was limited by its lack of strength; most polyimide-based microelectrode arrays bend easily and deviate from the desired implant site during implantation. Although the microelectrode arrays may be strengthened by adopting a thicker polyimide, the thicker device may cause greater harm to the tissue.

Neural signals with low signal-to-noise ratio (*SNR*) reduce spike detection and sorting accuracy. Although several powerful algorithms may be used to detect and sort spikes under low *SNR* conditions (Nenadic and Burdick, 2005), reducing electrode's impedance to increase *SNR* would further improve accuracy of the results. Because impedance is proportional to both thermal noise and signal loss through shunt pathways (Cheung, 2007; Ludwig et al., 2006), *SNR* would be improved with reduced impedance. Accordingly, signal loss would also be reduced. Therefore, some research coated electrode sites with conductive polymers, such as polypyrrole (PPy) (Cui et al., 2001) and poly (3,4-ethylenedioxythiophene or PEDOT) (Ludwig et al., 2006), to reduce electrode impedance. Besides additional coatings, Paik et al. (2003) found a trade-off relationship between electrode impedance and an electrode's effective surface area. Increasing the geometric area of an electrode may be the most intuitive way to increase its effective surface area. However, for any given length of microelectrode array, electrodes with larger geometric areas have lower recording site densities than those with smaller geometric areas. Furthermore, electrodes with a small geometric area isolate the single-unit activity from more distant units, thus improving single-unit selectivity (Ludwig et al., 2006; Paik et al., 2003). To maintain a high recording site density on microelectrode arrays, special and complicated fabrication methods have been developed to roughen the surface of the electrodes and increase their effective surface areas (De Haro et al., 2002; Lee et al., 2002; Paik et al., 2003).

Lesion marking of the tissue by electrolytic lesion indicates the physiological event of interest and identifies the precise anatomical location of the event. Electrolytic lesions have been shown to successfully mark the location of electrode sites in neural tissue after neural recordings (Brozoski et al., 2006; Townsend et al., 2002). Direct current (DC) was passed through the electrode, causing an irreversible electrochemical reaction that removed the metallic ions from the electrode surface (Branner et al., 2004; Lee et al., 2002). However, the inevitable increase in electrode impedance after electrolytic lesions (De Haro et al., 2002) would result in low quality neural signals or even recording failure (Branner and Normann, 2000). Designing a microelectrode array that could maintain high signal recording quality after repeated electrolytic lesions has become one of the most important issues in recent neurotechnology research and development.

Table 1
Specifications of the NCTU probe.

Parameter	Value
Number of sites	16
Probe length (A) (mm)	18.8
Probe width (B) (mm)	2
Shaft length (C) (mm)	14.9
Max shaft width (D) (μm)	996
Shaft width (E) (μm)	220
Tip width (F) (μm)	3
Distance (G) (μm)	48.4
Site radius (H) (μm)	16
Wire width (I) (μm)	10
Wire width (J) (μm)	5
Electrode distance (K) (μm)	74
Recording length (L) (mm)	1.1

A new microelectrode array, the NCTU (National Chiao Tung University) probe, was presented in the current study. The thin, tough and flexible polyimide-based substrate caused less harm to tissue at the implant site, enabling precise implantation. The roughened three-dimensional (3D) surface created with a simple microfabrication process furnished the electrode with a large effective surface area and low impedance during *in vivo* measurement. The electrode's DC tolerance for repeated electrolytic lesion was also increased by its thickness. Furthermore, results from chronic recording sessions showed high *SNR* neural signals and small electrode impedance variations.

2. Materials and methods

2.1. Fabrication of the NCTU probe

AutoCAD (AutoCAD 2002, Autodesk Inc., USA) was used to plot the main elements of the NCTU probe: the integrated connector pads, the long shaft and the electrode sites. The respective specifications were listed in Table 1 and depicted in Fig. 1.

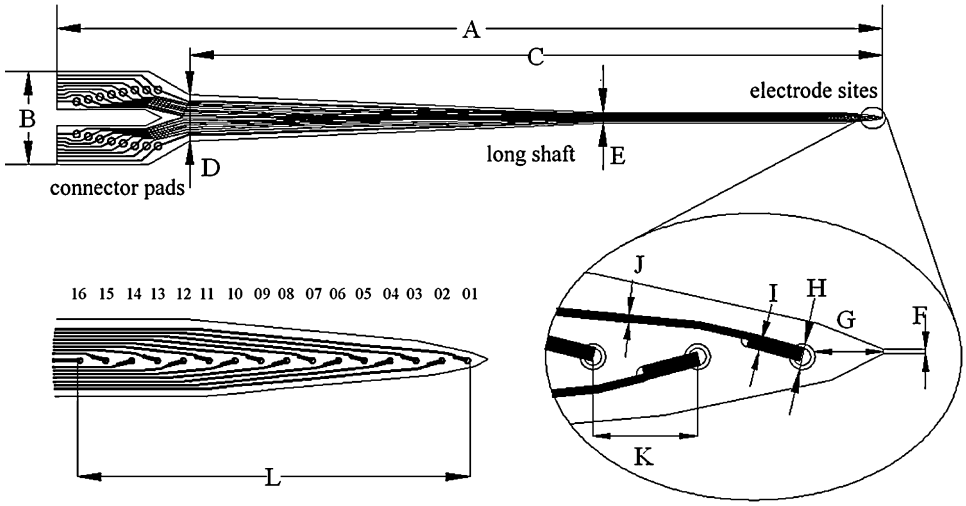

Fig. 1. Schematic view of the NCTU probe depicted in an AutoCAD layout (not drawn to scale). The probe was constructed with integrated connector pads, a long shaft and recording sites. The tip of the probe was designed with a 50° tapered angle. Dimensions were defined in Table 1.

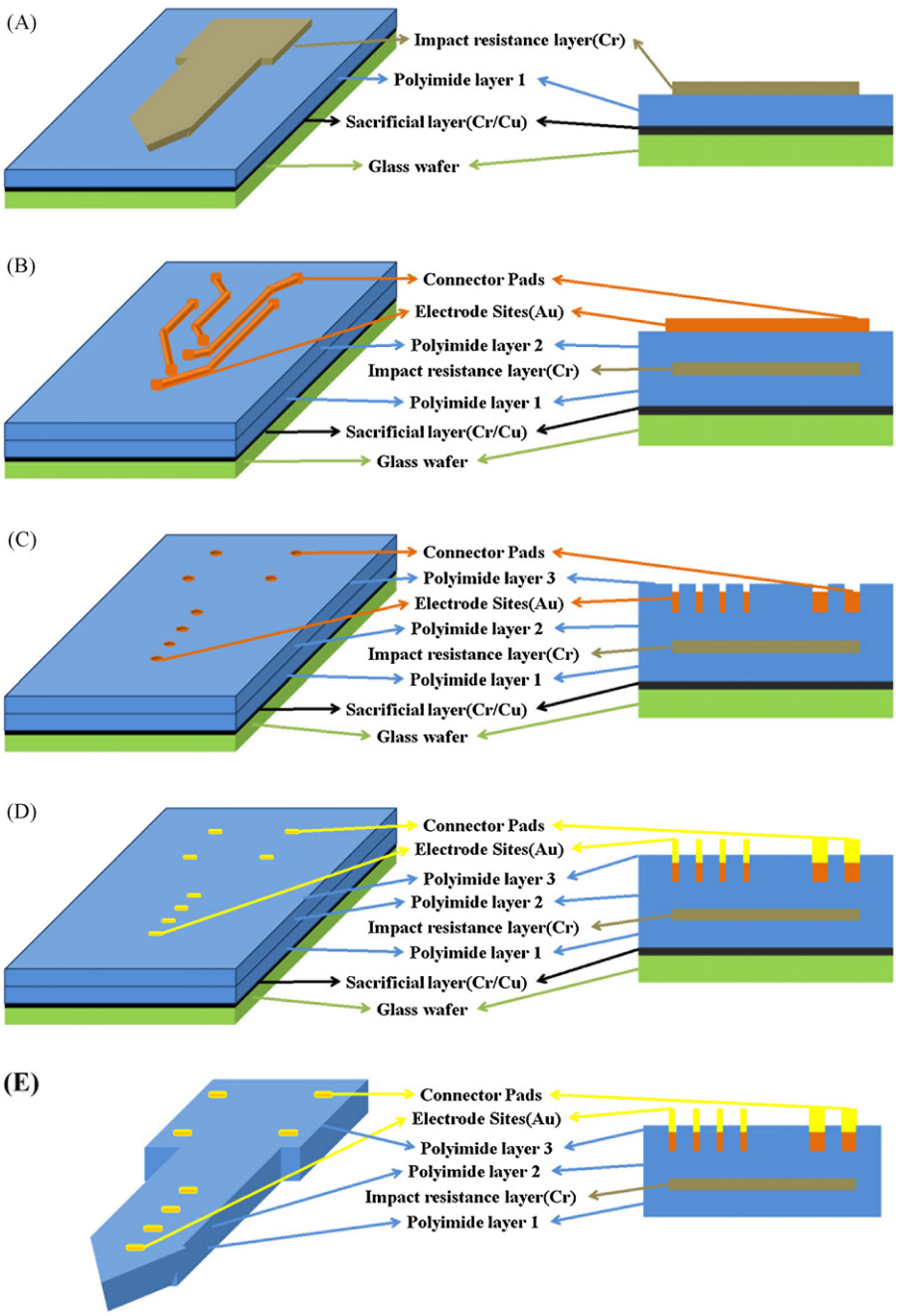

Fig. 2. An illustration of the fabrication process of the NCTU probe (not drawn to scale). (A) Impact-resistance layer was formed on the first 30-μm polyimide layer. (B) The trace layer was patterned on the second 30-μm polyimide layer, which was then etched to construct the 16 pairs of electrode/connector pads and interconnect traces. (C) The protective polyimide layer (3.2 μm) was spun onto the trace layer; windows for the 16-paired sites of electrode/connector pad were opened. (D) Gold was added by electroplating to form the 3D recording sites and connector pads. (E) The probe was outlined and detached.

Three masks were used in the fabrication process for the NCTU probe. The first mask (MASK #1) was used to construct the site bases of the electrode/connector pads and the interconnecting traces of the NCTU probe. The second mask (MASK #2) formed the 3D recording electrodes and connector pads. The third mask (MASK #3) was used to shape the NCTU probe, including the shaft and the angle of its tip. First, a 200 nm-thick chrome layer, followed by a 700 nm-thick copper layer, were sputtered (Vvs-70L, VICTOR Taichung Machinery Works Corp., Ltd., Taiwan) as the sacrificial layer onto a glass wafer. Next, a 30 μm-thick polyimide (PI-2611, HD Microsystems, USA) layer was coated onto the sacrificial layer with a spin coater (Model KW-4A, CHEMAT Technology, Inc., Taiwan); it was then cured for 30 min in an inert gas oven at 350 °C (QHMO-2, CSUN MFG. Ltd., Taiwan).

The impact resistance layer of the NCTU probe was created by depositing a 200 nm-thick chrome layer onto the cured polyimide. After the photoresistor (EPG512, Everlight Chemical Industrial Corp., Taiwan) was spun onto the impact resistance layer, MASK #3 was aligned and exposed. Chrome etchant (eSolv EG-201, Demand International Corp., Taiwan) was used to pattern the outline of the NCTU probe, as shown in Fig. 2A.

The trace layer was shown in Fig. 2B. A second polyimide layer (30 μm-thick) was coated on and cured as before. Next, a 100 nm-thick chrome layer and a 700 nm-thick copper layer were sputtered onto the second polyimide layer with a reactor. MASK #1 was used

to pattern the metal circuits, the 16 pairs of electrode/connector pads and the interconnecting traces lithographically. Chrome and copper were then respectively etched with chrome etchant (eSolv EG-201, Demand International Corp., Taiwan) and copper etchant (RTE-Cu29 WBL-B, Resound Tech. Inc., Taiwan), forming the structures of the metal circuits.

Next, the insulation procedure was carried out. A thin, third layer of polyimide (3.2 μm) was spun onto the trace layer for the protection of the metal circuits. Windows (3.2 μm) lithographically patterned with MASK #2 were created (O_2 plasma etching) on the third layer of polyimide, forming the 16 electrode/connector pad pair sites (Fig. 2C).

The 3D electrodes and connector pads were created with electroplating. Optimal electroplating parameters and control procedures were used to refine the structure of the electrodes and connector pads. Then, a 5 μm gold layer was deposited onto the electrode sites and connector pads (Fig. 2D).

The outline of the NCTU probe was lithographically patterned with MASK #3, which was etched with O_2 plasma. The sacrificial layer was selectively etched with copper etchant (RTE-Cu29 WBL-B, Resound Tech. Inc., Taiwan) in the final stage of fabrication. Finally, the NCTU probe was removed from the glass wafer (Fig. 2E). The fabricating procedures of the NCTU probe were shown in Fig. 2.

2.2. Subjects

The study, approved by the Institutional Animal Care and Use Committee at the National Chiao Tung University, was conducted according to the standards established in the Guide for the Care and Use of Laboratory Animals. Five male Wistar rats weighing 250–300 g (BioLASCO Taiwan Corp., Ltd.) were individually housed on a 12 h light/dark cycle, with access to food and water *ad libitum*.

2.3. Surgical implantation procedures

The animals were anesthetized with pentobarbital (50 mg/kg i.p.) and placed on a standard stereotaxic apparatus (Model 900, David Kopf, USA). The implantation site and reference screws were demarcated. Holes were then drilled through the skull of the rat. Stainless steel bone screws were inserted into the skull, and the cortical surface was irrigated with phosphate buffered saline (PBS). After the dura was removed from the brain, the NCTU probe was inserted vertically into the thalamic ventral posterior medial (VPM) nucleus (target location: P 3.6 mm and L 3.2 mm with respect to the bregma, 5.6 mm from the surface of the brain); Paxinos and Watson's (2007) atlas was used as a reference. The NCTU probe, four stainless steel bone screws, and the connector were permanently cemented to the bone with dental acrylic (Type 1 Class 1, Hygenic Corp., USA). During probe implantation, the animals' blood pressures were maintained at > 90 mm Hg, with 3–4.5% end tidal CO_2 concentration. The animals were given a one-week post-surgery recovery period, after which neural signals were recorded every two days for six weeks.

2.4. Neural ensemble recording and SNR analysis

During the recording sessions, the animal was free to move within the recording booth while neural signals were recorded continuously for 5 min. A Multi-Channel Acquisition Processor (MAP, Plexon Inc., USA) was used to record neural signals from the 16-channel NCTU probe. The recorded electrical signals were transmitted from the headstage to an amplifier, through a band-pass filter (spike preamp filter: 450–5 kHz; gain: 15,000–20,000), and sampled at 40 kHz per channel.

Chebyshev's theorem was used to set the threshold to determine the presence of spikes in the sample. It was stated that the probability that any random variable, X, will assume a value within k standard deviations of the mean is at least $1-1/k^2$. In some research, the thresholds were set between three and five standard deviations (SD) to detect action potentials (Ludwig et al., 2006; Snider and Bonds, 1998; Vetter et al., 2004). In this study, the threshold was set at four SD above or below the mean noise level. That is, in the absence of spike activity, at least 93.75% of the signals would fall within the threshold. Spikes from each electrode were classified with template sorting algorithms in a commercial software (Offline Sorter, Plexon Inc., USA); single units were identified and isolated from the recorded neural signals.

The quality of neural signals recorded was analyzed offline with *SNR* estimation in MATLAB (MATLAB R11, Mathworks Inc., USA). The present study defined *SNR* as the root mean square of background noise to the average peak-to-peak amplitude of spikes (Maynard et al., 2000; Ludwig et al., 2006). *SNR* estimation was conducted as follows:

First, the 5-min neural signal, X_t, was divided into L segments of 30-s, x_i, where $1 \le i \le L$ (in this study, $L = 10$). k was defined as the number of data points in x_i, with mean, $\bar{x}_i$. The threshold, Th_i, was determined by the distribution probability of the 30 s/segment neural signal x_i. Th_i was set to 4 SD for x_i,

$$X_t = (x_1, x_2, \ldots, x_L)$$

$$Th_i = 4 \cdot \sqrt{\frac{1}{k-1}\sum_{j=1}^{k}(x_i(j) - \bar{x}_i)^2}$$

Next, Th_i was used to detect spikes from each segment x_i,

$$\begin{cases} x_i \in s_i & \text{, if } x_i \ge \pm Th_i \\ x_i \in n_i & \text{, else} \end{cases} \Rightarrow \begin{cases} \tilde{S}_i & \text{: spikes in } x_i \\ \tilde{N}_i & \text{: background noise in } x_i \end{cases}$$

Finally, *SNR* was estimated as

$$AVG(PP(\tilde{S}_i)) = \frac{1}{m_i}\sum_{p=1}^{m_i} PP(\tilde{S}_i^p)$$

$$rms(\tilde{N}_i) = \sqrt{\frac{1}{o_i}\sum_{q=1}^{o_i}(\tilde{N}_i^q)^2}$$

$$SNR_i = \frac{AVG(PP(\tilde{S}_i))}{2 \times rms(\tilde{N}_i)}$$

$$SNR = \frac{1}{L}\sum_{i=1}^{L} SNR_i$$

where $PP(\tilde{S}_i)$ was the peak-to-peak spike amplitude in $\tilde{S}_i$, m_i was the number of spikes in $\tilde{S}_i$, $rms(\tilde{N}_i)$ was the root mean square of the background noise, $\tilde{N}_i$, and o_i was the number of data points in $\tilde{N}_i$.

2.5. Measurements of in vitro and in vivo electrode impedance

The impedance of each electrode on the NCTU probe was measured with an impedance spectroscopy (LCR4235, Wayne Kerr Electronics Ltd., UK). Immersed in PBS solution, *in vitro* impedance of the NCTU probe and a large Ag/AgCl reference electrode was measured by applying a 10 Hz to 10 kHz 20 mV sinusoidal voltage.

In vivo impedance was measured in animals with implants every two days for six weeks after the one-week recovery period. Impedance of the 16 implanted electrodes were measured with a sinusoidal voltage source (20 mV, <150 nA, at 1 kHz).

2.6. Histological procedures

After the last recording session, each rat was anesthetized with sodium pentobarbital (50 mg/kg, i.p.). A 30 μA DC was directed

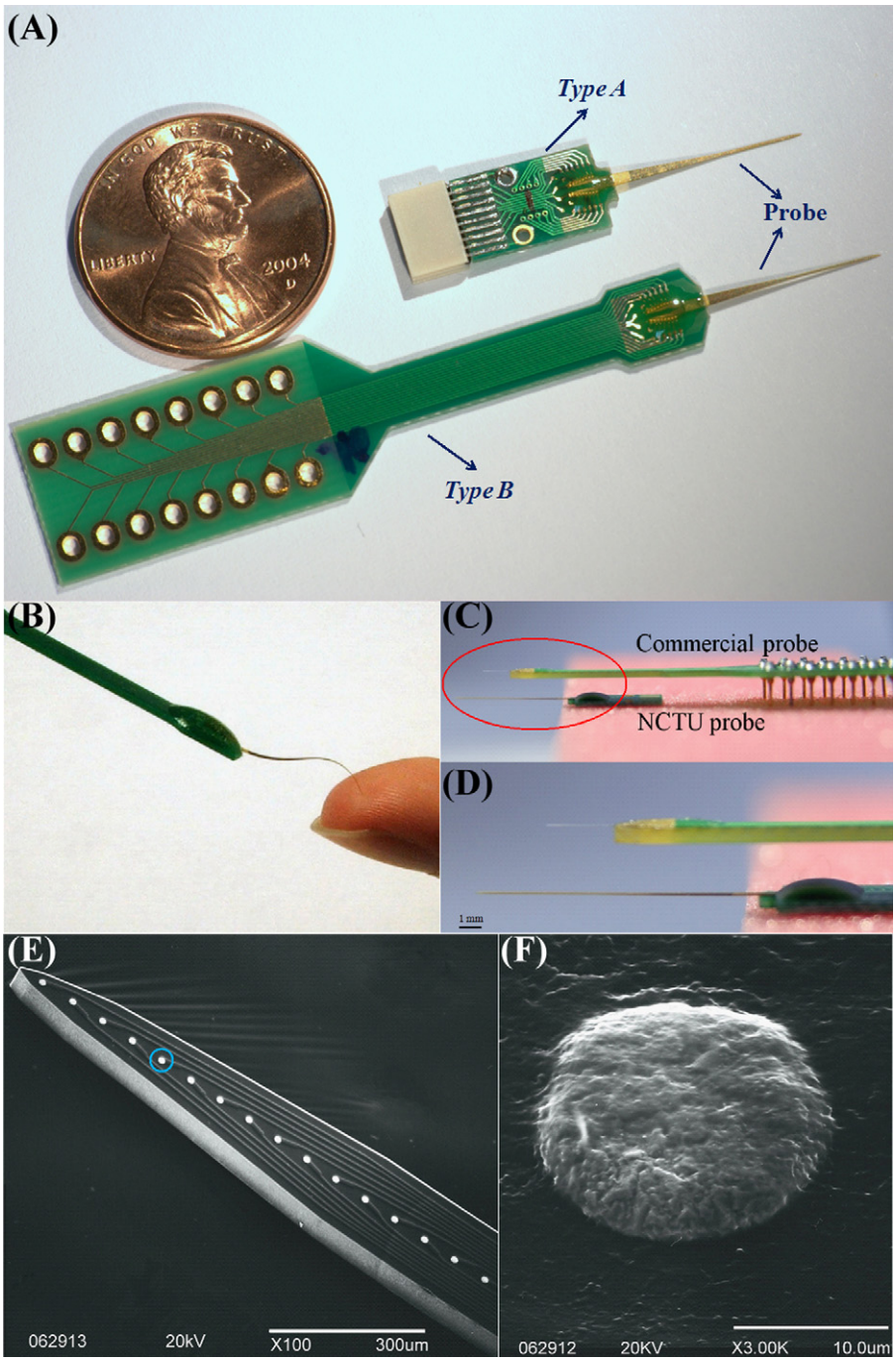

Fig. 3. An overall view of the NCTU probe assembly and SEM images of the electrodes. (A) The NCTU probe was bonded onto two different types of PCB. *Type A* assembly was used for chronic recording and *Type B* was used for acute recording in free-moving animals. (B) The NCTU probe was flexible; its original shape was restored even after it was severely bent. (C) In contrast to the shaft of a commercial probe, the long NCTU probe shaft did not bend when positioned horizontally. (D) SEM image of the NCTU probe with 16 recording sites. (E) An enlarged SEM image of the electrode in the blue circle, indicating a 3D structure with rough surface.

to the outermost site of the NCTU probe for 10 s (Cheung et al., 2007), marking the specific recording site in the brain with an isolated pulse stimulator (Model 2100, A-M Systems Inc., USA). The rats were then given an overdose of anesthetic and perfused with a mixture of 150 ml ice-cold PBS solution and 500 ml 4% paraformaldehyde at the flow rate of 50 ml/min. The brains were carefully removed from the skulls and kept in a mixture of 4% paraformaldehyde and 30% sucrose at 4 °C for two days. Afterwards, each brain was sliced into 50-μm coronal sections with a freezing microtome (CM 1800, Leica, Germany). In order to identify the brain tissue and confirm the recording locations, both neurons and glia in the tissue sections were stained blue/violet with 0.1% cresyl violet.

2.7. Electrodes' tolerance for electrolytic lesions and direct current

Two tests were conducted to evaluate electrodes' DC tolerance. The first test examined the maximum number of electrolytic lesions the electrode could withstand. Repeated electrolytic lesions were induced in the rat brain with a constant anodal current (30 μA, 10 s). After each electrolytic lesion, the probe was carefully removed and immersed in PBS solution for *in vitro* impedance (at 1 kHz) measure-

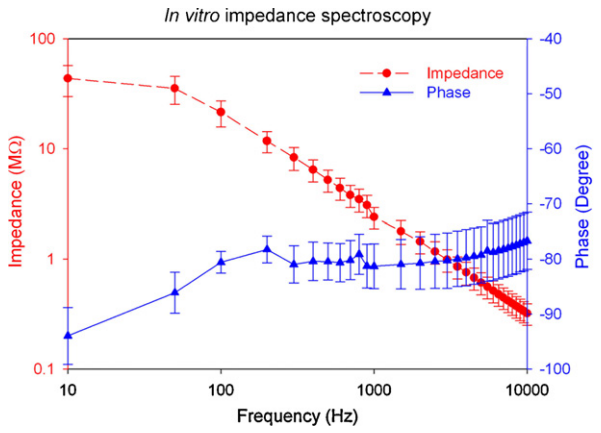

Fig. 4. The impedance spectroscopy of NCTU probe, with the impedance spectrum and the phase spectrum ranging from 10 Hz to 10 kHz. The average impedance was 2.40 MΩ ± 0.52 MΩ at 1 kHz.

ment. The procedures were repeated until a drastic increase in the electrode impedance was observed, indicating that the electrode was no longer functional.

The second test was administered to determine the largest DC that the electrode could tolerate. Each 10 s anodal DC (50, 100, 200, 500 μA, 1, 2, 5 and 10 mA) was conducted through the electrode three times, after which *in vitro* impedance was measured as in the first test.

3. Results

3.1. NCTU probe assembly

Two types of NCTU probe assemblies, *Type A* for implantation and *Type B* for chronic recording, were respectively constructed (Fig. 3A). *Type A*: the NCTU probe was bonded onto a miniature printed circuit boards (PCB) that was combined with a connector (A8141-001, Omnetics Connector Corp., USA). The small and light (<3 g) assembly could be implanted into the rat brain, allowing the animal to move freely. *Type B*: the NCTU probe was wire-bonded onto a standard Dual-Inline Pin (DIP) PCB, with pins soldered into two rows of 8 in a wide DIP format. An adapter (ADP/8o50-MICH, Plexon Inc., USA) was applied as an interface between the Plexon headstage and the *Type B* assembly for acute recording.

As shown in Fig. 3B, the original shape of the probe was restored even after it was bent at the tip. The NCTU probe and the commercial probe (No. a1 × 16-3mm50-177, NeuroNexus, USA) were juxtaposed in Fig. 3C. As shown in the enlarged image of Fig. 3C (circled in red), the NCTU probe's longer shaft stretched as straight as the commercial probe with no downward slant (Fig. 3D). Young's modulus is a measure of the stiffness of an isotropic elastic material. The Young's modulus of the NCTU probe was 54 GPa. Scanning electron micrograph (SEM) images of the NCTU probe were displayed in Fig. 3E and F. In Fig. 3E, the 16 electrode sites and interconnecting traces based on the long shaft of polyimide substrate were shown. The enlarged image of Fig. 3E (circled in blue) presented the rough 3D structure of the electrode (Fig. 3F).

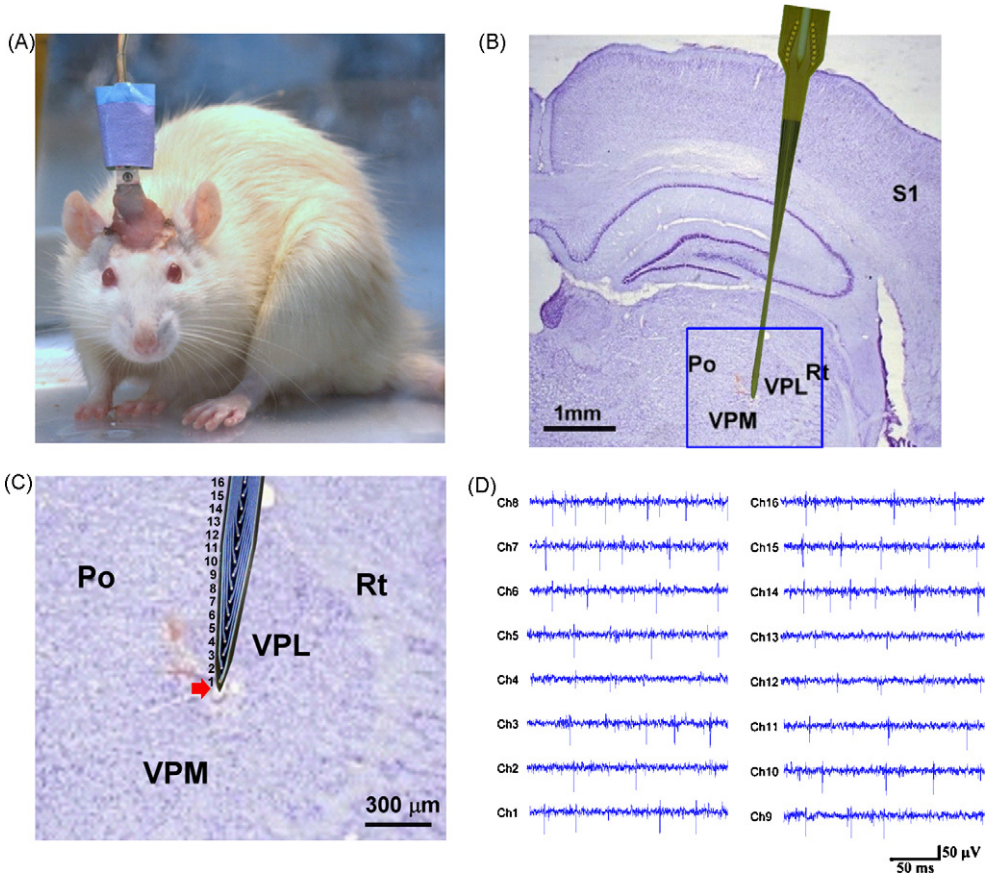

Fig. 5. Neural ensemble recordings in a free-moving rat. (A) A normally behaving rat implanted with a 16-channel NCTU probe, connected to a Plexon headstage and cables. (B) Photomicrograph of a Nissl-stained coronal section at the anteroposterior (AP) level of −3.6 mm relative to the bregma. The *in situ* location of the NCTU probe was also shown. S1, primary somatosensory cortex; Po, the posterior thalamus nuclear group; Rt, reticular thalamus nucleus; VPM, ventral posteromedial thalamus nucleus; VPL, ventral posterolateral thalamic nucleus. (C) An enlarged photomicrograph of the blue rectangle in (B) indicated the implantation location in the thalamus. A reference lesion site (red arrowhead) in the VPM, was observed at the depth of 5600 μm. (D) Four weeks after implantation, the 16-channel neural activities were simultaneously recorded from the VPM of a freely moving rat.

3.2. In vitro impedance spectroscopy

As the quality of neural signal recording is affected by electrode impedance, electrode impedance was examined in this section. The *in vitro* impedance of the 16 electrodes on the NCTU probe, measured by impedance spectroscopy, was illustrated in Fig. 4. The phase of the electrodes was approximately −80° after 100 Hz. A gradual decline in the magnitude of impedance was found with increased frequency. The *in vitro* impedance of one NCTU probe was 2.40 ± 0.52 MΩ (mean ± SD, $n = 16$), with a −81° phase at 1 kHz.

3.3. Neural ensemble recording: in vivo impedance and SNR estimation

The NCTU probe was primarily designed for chronic recording. A normally behaving rat, implanted with the *Type A* assembly probe, was shown in Fig. 5A. This small NCTU probe assembly allowed the rat to move freely in different situations, such as running, exploring, eating, grooming, sleeping, and performing learned tasks. The VPM was classified as a subcortical relay station of the lemniscal pathway, receiving somatosensory information from whisker follicles and gathering tactile information about the environment (Sugitani et al., 1990). Accordingly, neural signals were recorded from the VPM during unrestrained behavior. A photomicrograph of the implantation section was shown in Fig. 5B. The figure was modified by superimposing one lesion marker on one implantation track, which was then overlaid with a scaled image of the NCTU probe. The lesion marker (arrowhead, with a vertical diameter of approximately 80 μm) was used to identify the location of the outermost recording site. The recording site, in relative to the VPM, was shown in the enlarged photomicrograph of the area (the blue rectangle) (Fig. 5C). The spontaneous neural activities simultaneously recorded from the 16 electrodes during the fourth week of implantation were shown in Fig. 5D.

After implantation, *in vivo* impedance (at 1 kHz), *SNR* of the implanted NCTU probe and the number of units per channel over time, were measured (Fig. 6). *In vivo* impedance (at 1 kHz) was measured to detect chronic tissue proliferation around the electrodes (Suner et al., 2005). After implantation (Day 0), the probe's *in vivo* impedance (at 1 kHz) was 0.61 ± 0.14 MΩ (mean ± SD, $n = 16$). During the first two weeks of implantation, the *in vivo* impedance increased slightly, attaining a maximum of 0.70 ± 0.09 MΩ on the 14th day. Afterwards, the *in vivo* impedance curve gradually sloped downward into flatness *SNR* results estimated the quality of neural signal recordings over time. The *SNR* of recorded signals ranged from 4 to 5, with no significant decrease within the entire recording session (Fig. 6). In all the five animal subjects, the number of viable electrodes ranged from 98% to 100% (average of 97.5%). Multi-unit and single-unit were recorded from the 16-channel NCTU probe over time. On the 0th day, 1.31 ± 0.48 units/channel (mean ± SD) were recorded from one animal; monitoring results for 50 days were shown in Fig. 6. Although the number of units varied, there was no decrease over time. Results indicated that the NCTU probe was stable for at least 40 days.

3.4. Surface microstructure of the NCTU probe electrode

Atomic force microscopy (AFM) was used to evaluate the surface topography of the NCTU probe electrode and measure the roughness of the surface. The 2D surface topography of an electroplated electrode was shown in Fig. 7A. Image dimensions were 25 μm × 25 μm, with 128 scan lines. Vertical dimensions along the 64th scan line were shown in Fig. 7B. A large height variation was observed (between the two red arrowheads), where the diameter of the electrode was 15.62 μm. The 3D surface topography (Fig. 7C) was reconstructed from the 128 scan line profiles in Fig. 7A. The

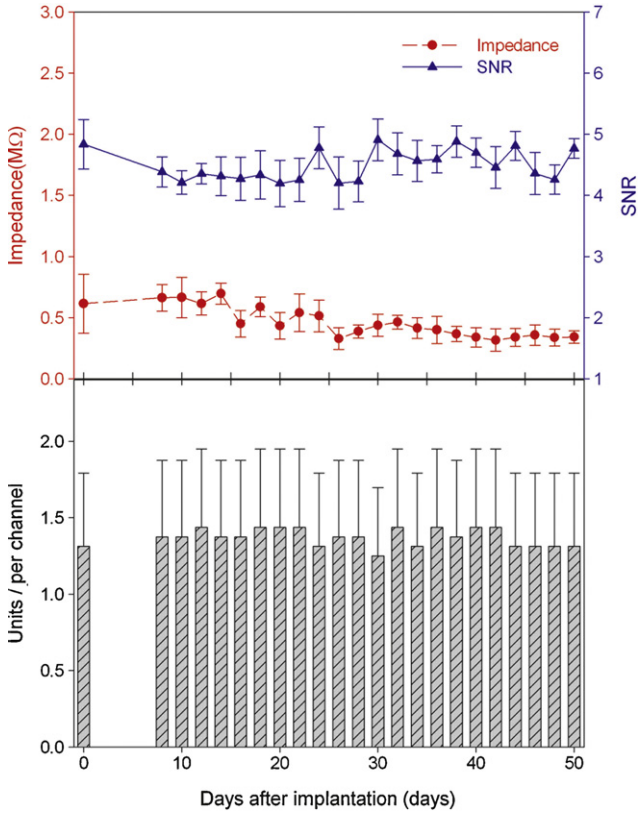

Fig. 6. Mean *in vivo* impedance magnitudes of the electrodes at 1 kHz, mean *SNR* of recording signals from the electrodes, and the mean number of units from the channel across recording sessions. Impedance, *SNR*, and activity units were measured every two days after the one-week recovery period.

vertical distance of the 3D surface ranged from 0.69 μm (Z_{max}) to −0.80 μm (Z_{min}), with an average of 0.80 μm (Z_{avg}). The surface of the electrode had an average roughness (R_a) of 0.21 μm and a root-mean-square roughness (R_{RMS}) of 0.27 μm. With an uneven surface topography and a geometric area of 625 μm^2, the surface of the electrode was increased to 697 μm^2.

3.5. Comparison of electrode DC tolerance between the NCTU and commercial probes

The electrodes' DC tolerance reflects the robustness of the electrodes following repeated electrolytic lesions. After a 30 μA DC was directed through the outermost electrode for 10 s, *in vitro* impedance of electrodes on the NCTU probe and the commercial probe were measured (Fig. 8A). Results showed that *in vitro* impedance of the NCTU probe remained within the normal range (~0.67 MΩ) even after 60 electrolytic lesions. In contrast, *in vitro* impedance of the commercial probe showed a substantial increase from 0.68 to 13 MΩ after the 34th DC lesion, an indication of electrode malfunction. As shown in Fig. 8B, the electrode surface on the commercial probe broke down after the 39th DC lesion. Meanwhile, the SEM image in Fig. 8C showed that the electrode on the NCTU probe was still intact after the 60th DC lesion.

To evaluate the DC tolerance limit of the NCTU probe's electrodes, DC of different intensities were directed through the electrodes. The procedure began from the smallest DC intensity; each DC was repeated 3 times before intensity was increased. The change in *in vitro* impedance after the conduction of DC was presented in Fig. 9A. Initial impedance, prior to electrolytic lesion, was 1.61 MΩ (denoted with arrowhead). Results showed *in vitro* impedance varied when DC intensities of 50, 100, 200, 500μA,

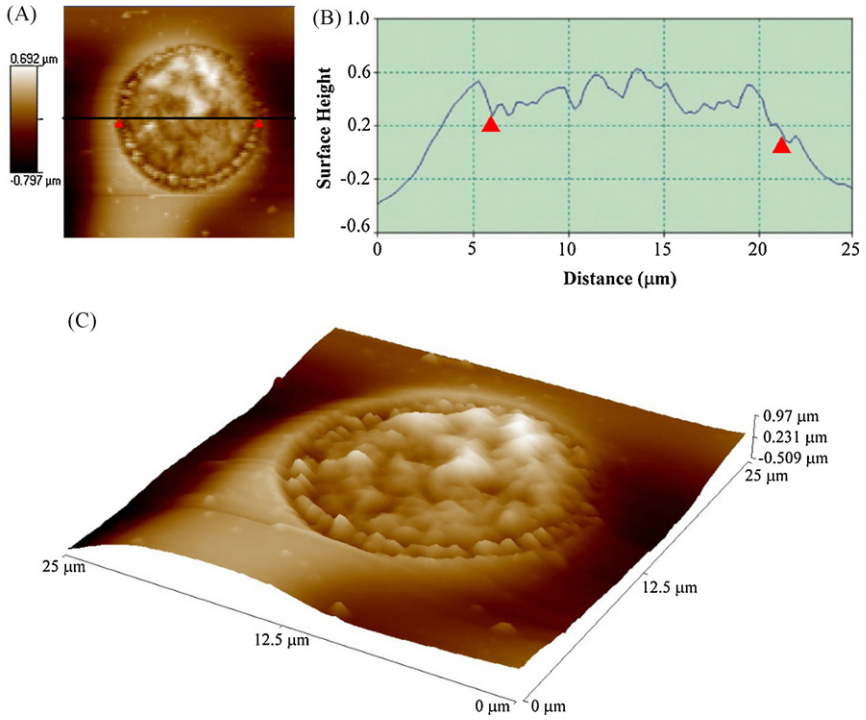

Fig. 7. *In situ* AFM experiment performed on an electroplated electrode on the NCTU probe. The AFM image (A) of the electrode topography with scanning dimension of 25 μm × 25 μm. The dark colors indicated the lowest points, while the bright colors indicated the highest points of the topography. (B) Section analysis along the black line in (A) indicated the profile and diameter (between 2 arrowheads) of the electrode. (C) A 3D AFM image of the electrode. (For interpretation of the references to color in this figure legend, the reader is referred to the web version of the article.)

1, 2, 5 and 10 mA were induced through the electrode. However, impedance showed a significant increase from 1.43 to 8.45 MΩ after a 10 mA anodal current was induced. After the third time, the outermost electrode on the NCTU probe broke and its polyimide film peeled off from the base (Fig. 9B).

Results indicated the electrode on the NCTU probe could tolerate as many as 60 electrolytic lesions, and a maximum of 5 mA DC for 10 s.

4. Discussion

A flexible, polyimide-based microelectrode array applicable for chronic recording was presented in this study. Metallic layers were sandwiched between polyimide layers to strengthen the NCTU probe and increase the precision of implantation. Results from *in vivo* impedance and *SNR* variation indicated the NCTU probe presented stable and quality chronic recording could. In addition, the sturdiness, density and thickness of each electrode were effectively increased by electroplating, thus extending the lifespan for signal recordings and electrolytic lesions.

4.1. The strengthened NCTU probe

Recent studies have applied silicon-based microelectrode arrays in chronic neural signal recordings (Bai et al., 2000; Csicsvari et al., 2003; Tae Hwan et al., 2000). However, micromotion at the tissue–electrode contact areas induced persistent inflammatory responses (Cheung, 2007), directly resulting in neuronal loss. After a certain period, the efficiency of signal recordings may also be affected (Polikov et al., 2005; Szarowski et al., 2003). Prior studies suggested that polyimide-based microelectrode arrays, with a small Young's modulus (~3 GPa) as compared to silicon (~170 GPa), have gained increasing popularity in research and development (Cheung et al., 2007; Lee et al., 2004b; Subbaroyan et al., 2005). As the Young's modulus difference between the microelectrode array and brain tissue is small, inflammatory responses during long-term implantation was reduced, hence improving the stability during chronic recordings (Cheung, 2007; Kim et al., 2004; Ludwig et al., 2006). However, a microelectrode array constructed from a polyimide-based substrate was easily bent and deviated from the desired implant site during the implantation.

Although there were attempts to improve polyimide-based microelectrode arrays by optimizing the use of several metallic materials, microelectrode arrays available were not sturdy enough, and their shafts were not applicable for deep brain implantation. Rousche et al. (2001) constructed a microelectrode array by sandwiching a gold layer (200 nm-thick) between two layers of polyimide (10–20 μm-thick). However, this microelectrode array was too soft to be inserted directly into brain tissue; an incision was required for implantation. As an alternative option, a tungsten wire (~100 μm) could be used to guide the implantation. Nevertheless, the microelectrode array was only long enough to reach the cortex. Another microelectrode array was fabricated with two Ti/Pt (50 nm/200 nm) electrode layers, separated with a polyimide layer (Cheung et al., 2007). Using this microelectrode array, the hippocampus could be reached without an implantation guide. However, the microelectrode array substrate was not strong enough; deep brain implantation resulted in the bending of the shaft. The NCTU probe presented in this article reduced the microelectrode array's micromotion against tissue at the implantation site, and also allowed precise insertion into the anatomical area of interest without bending.

An impact resistance layer was applied to the NCTU probe to increase its strength. It was constructed by sandwiching a 200 nm-thick chrome layer between two 30 μm-thick polyimide layers. This design increased the strength of the polyimide-based microelectrode array while retaining the flexibility. In order to construct a microelectrode array that is long enough to penetrate into the deep brain without bending or path deviation, materials with a certain amount of strength was required. The Young's modu-

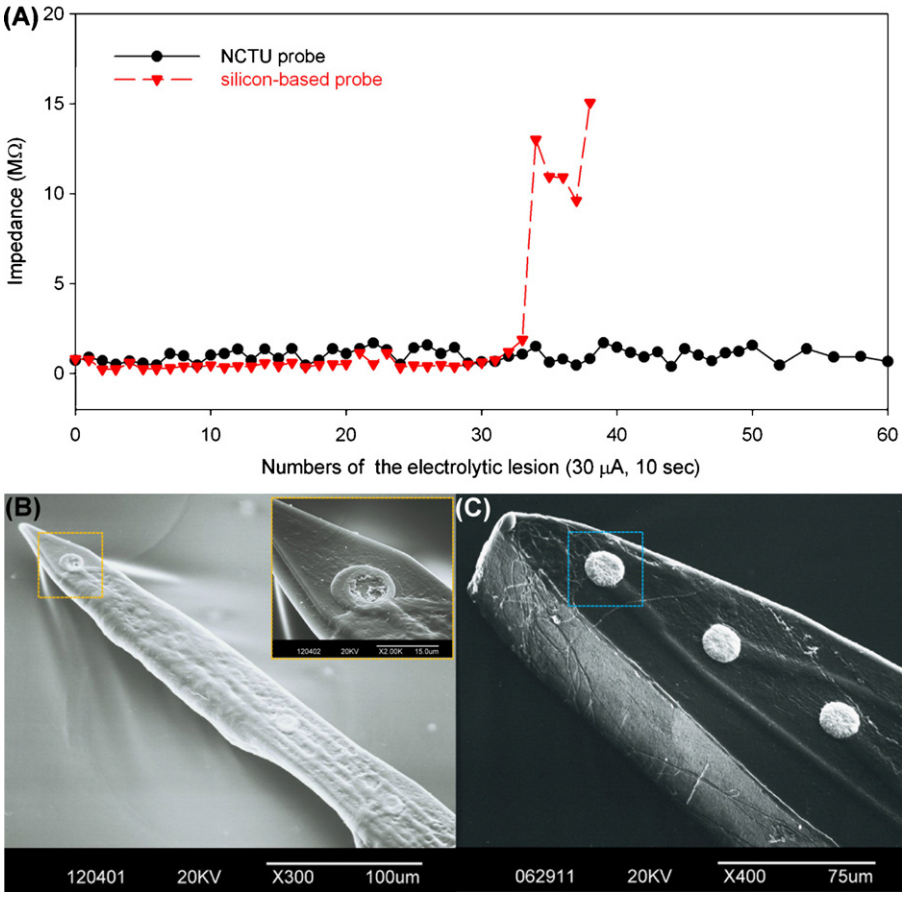

Fig. 8. The maximum number of repeated electrolytic lesions tolerated by electrodes on the NCTU probe and the commercial probe. (A) *In vitro* impedance of the electrode was measured after a number of electrolytic lesions. (B) An enlarged SEM image of the outermost electrode on the commercial probe, as indicated in the yellow rectangle; it was corroded after the 39th electrolytic lesion. (C) SEM image of the outermost electrode on the NCTU probe, as indicated in the blue rectangle; it remained intact after 60 electrolytic lesions.

lus of the NCTU probe was increased to 54 GPa, falling within that of silicon-based microelectrode array (~170 GPa) and purely polyimide-based microelectrode array (~3 GPa). Consequently, harmful effects caused by micromotion at the tissue–electrode contact area were reduced, and the NCTU probe could be inserted directly into deep brain. The NCTU probe showed improvement from brittle, silicon-based (Cheung et al., 2003; Rousche and Normann, 1999; Suner et al., 2005) and some soft polyimide-based microelectrode arrays (Cheung et al., 2007; Rousche et al., 2001). Results from this study demonstrated significant advantages in applying the NCTU probe to chronic implantation.

4.2. Quality and stable chronic recording

A two-phase transition of *in vivo* impedance (at 1 kHz) was found for the electrode on the NCTU probe during the recording session (Fig. 6). For the first two weeks of implantation, *in vivo* impedance increased, which then decreased at the third week. Bio-film encapsulation around the implant, caused by immune responses, could affect *in vivo* impedance (Vetter et al., 2004; Ludwig et al., 2006). In our study, *in vivo* impedance showed a steady increase until the 14th day of recording, a result from acute immune responses. At this stage, the microelectrode array insertion damaged the brain tis-

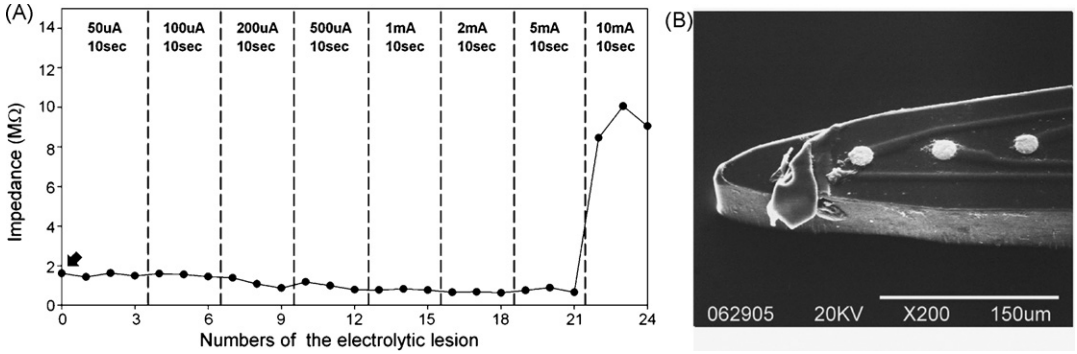

Fig. 9. DC tolerance of electrodes on the NCTU probe (A) *In vitro* impedance of the electrode was measured after electrolytic lesion at various DC intensities. Initial impedance (black arrowhead) was 1.61 MΩ. (B) SEM image of the broken electrode; a polyimide film peeled off the probe substrate after a 10 s, 10 mA electrolytic pulse.

sue, inducing an initial wound healing response. Microglia, which was produced to repair the damaged area, eventually enveloped the electrodes, and gliosis insulated the electrodes from the signal source (Biran et al., 2005; Polikov et al., 2005). Chronic foreign body reactions against the microelectrode array then occurred, and reactive astrocytes (glial scar and activated microglia) began to distribute around the implant (Biran et al., 2005; Polikov et al., 2005; Szarowski et al., 2003; Turner et al., 1999). The second phase began after the 14th day of recording. As acute immune response activities decreased, *in vivo* impedance gradually decreased (Fig. 6). Such impedance changes were also found in studies using silicon-based electrodes (Ludwig et al., 2006; Vetter et al., 2004).

Suner et al. (2005) and Ludwig et al.'s (2006) *SNR* estimation methods were adopted in this study. Their work suggested that an *SNR* greater than 4 indicated a high quality signal. In Ludwig et al.'s (2006) study, *SNR* of the silicon-based microelectrode array ranged from 4 to 6. Across all recording sessions, *SNR* estimation results of the NCTU probe were between 4 and 5, implying the received signals were of good quality (Fig. 6). The small *SNR* variation suggested the NCTU probe was more stable than that used in Ludwig et al.'s (2006) study. Due to disparities among animal models, surgical techniques, and signal quality measurements, it was not feasible to compare microelectrode arrays used in different studies (Vetter et al., 2004). Therefore, it is reasonable to conclude that the NCTU probe produced high quality and stable chronic recordings.

On average, 97.5% of the electrodes retained their viability during the recording sessions of the five animal subjects (15/16 for two subjects, 16/16 for three subjects). The high retaining rate indicated the NCTU probe was highly reliable. The mean number of units showed no significant variance over time (Fig. 6). The relationship between the *SNR* of the NCTU probe and the number of units from the channel was not examined in this study. However, less multi-unit channels were recorded if the *SNR* of the NCTU probe was greater than 4.7.

4.3. Advantages of the electroplated electrode

Results from the AFM images and section analysis of the electrodes on the commercial probe (thin-film deposited; data available upon request) and the NCTU probe (electroplated) indicated that electroplating produced electrodes with rougher 3D surfaces. Electroplated electrodes showed high corrosion resistance and roughened surfaces (De Haro et al., 2002). The effective surface area was hence increased and electrode impedance was reduced (De Haro et al., 2002; Kovacs, 1994; Paik et al., 2003). Accordingly, our evaluations indicated that *in vivo* and *in vitro* impedance of the electroplated electrodes on the NCTU probe was smaller than those of the thin-film deposited electrodes on the commercial probe. Evaluated under the same criteria, *in vitro* and *in vivo* impedance values for the commercial probe at 1 kHz were $2.71 \pm 0.99\,M\Omega$ and $0.93 \pm 0.16\,M\Omega$, respectively.

Given that electroplating attained harder, denser and thicker deposits that could withstand a large amount of metal dissolution (De Haro et al., 2002), electrodes on the NCTU probe could tolerate stronger electrical conduction than those on the commercial probe. DC is usually passed through electrodes for lesion markings of tissue after neural signal recordings (Branner and Normann, 2000; Cheung et al., 2007; DiCarlo et al., 1996). A recent method used radiofrequency (RF) lesions to mark each of the 16 recording sites of a 16-channel linear array multiprobes (Brozoski et al., 2006). However, RF lesion methods were much less destructive than DC lesion methods (Brozoski et al., 2006; Townsend et al., 2002), electrode performance of the NCTU probe was thus examined with DC lesions. Having a high tolerance threshold for DC, the NCTU probe electrodes were also robust for RF current. As DC was passed through the electrode, electromigration (Arnaud et al., 2000) and thermomigration (Manku and Orchard-Webb, 1995) caused ion migration on the metallic thin-film. Repeated electrolytic lesions, therefore, reduced the thickness of the thin-film electrode, increasing electrode impedance that consequently caused structurally irreversible electrode malfunction (De Haro et al., 2002). The thin-film deposited electrodes on the commercial probe were shown to be more vulnerable than the electroplated electrodes on the NCTU probe. The hard, dense and thick electrodes on the NCTU probe were stable during chronic recording. Moreover, the application of the NCTU probe could reduce the replacement costs due to malfunction.

Results in this study indicated that the NCTU probe showed good biocompatibility, high and stable *SNR* for chronic recording, as well as great DC tolerance for electrolytic lesion or electrical stimulation. Therefore, the NCTU probe could serve as a useful device for future neuroscience research.

Acknowledgments

The authors thank Miss Pen-Li Lu (Institute of Biomedical Engineering, National Taiwan University) for her assistance with histological procedures. This study was supported by grants from the National Science Council of the Republic of China (NSC 95-2221-E-009-171-MY3) and the VGHUST Joint Research Program, Tsou's Foundation (VGHUST96-P5-19). The authors would like to contribute 20 free NCTU probes each year for academic research purposes; details are available upon request.

References

Arnaud L, Tartavel G, Berger T, Mariolle D, Gobil Y, Touet I. Microstructure and electromigration in copper damascene lines. Microelectron Reliab 2000;40:77–86.
Bai Q, Wise KD, Anderson DJ. A high-yield microassembly structure for three-dimensional microelectrode arrays. IEEE Trans Biomed Eng 2000;47:281–9.
Biran R, Martin DC, Tresco PA. The brain tissue response to implanted silicon microelectrode arrays is increased when the device is tethered to the skull. J Biomed Mater Res A 2007;82A:169–78.
Biran R, Martin DC, Tresco PA. Neuronal cell loss accompanies the brain tissue response to chronically implanted silicon microelectrode arrays. Exp Neurol 2005;195:115–26.
Branner A, Normann RA. A multielectrode array for intrafascicular recording and stimulation in sciatic nerve of cats. Brain Res Bull 2000;51:293–306.
Branner A, Stein RB, Fernandez E, Aoyagi Y, Normann RA. Long-term stimulation and recording with a penetrating microelectrode array in cat sciatic nerve. IEEE Trans Biomed Eng 2004;51:146–57.
Brozoski TJ, Caspary DM, Bauer CA. Marking multi-channel silicon-substrate electrode recording sites using radiofrequency lesions. J Neurosci Methods 2006;150:185–91.
Butovas S, Schwarz C. Spatiotemporal effects of microstimulation in rat neocortex: a parametric study using multielectrode recordings. J Neurophysiol 2003;90:3024–39.
Chen YY, Kuo TS, Jaw FS. A laser micromachined probe for recording multiple field potentials in the thalamus. J Neurosci Methods 2004;139:99–109.
Cheung KC. Implantable microscale neural interfaces. Biomed Microdevices 2007;9:923–38.
Cheung KC, Djupsund K, Dan Y, Lee LP. Implantable multichannel electrode array based on SOI technology. IEEE J Microelectromech Syst 2003;12:179–84.
Cheung KC, Renaud P, Tanila H, Djupsund K. Flexible polyimide microelectrode array for *in vivo* recordings and current source density analysis. Biosens Bioelectron 2007;22:1783–90.
Csicsvari J, Henze DA, Jamieson B, Harris KD, Sirota A, Bartho P, et al. Massively parallel recording of unit and local field potentials with silicon-based electrodes. J Neurophysiol 2003;90:1314–23.
Cui X, Lee VA, Raphael Y, Wiler JA, Hetke JF, Anderson DJ, et al. Surface modification of neural recording electrodes with conducting polymer/biomolecule blends. J Biomed Mater Res 2001;56:261–72.
De Haro C, Mas R, Abadal G, Munoz J, Perez-Murano F, Dominguez C. Electrochemical platinum coatings for improving performance of implantable microelectrode arrays. Biomaterials 2002;23:4515–21.
DiCarlo JJ, Lane JW, Hsiao SS, Johnson KO. Marking microelectrode penetrations with fluorescent dyes. J Neurosci Methods 1996;64:75–81.
Kim C-S, Ufer S, Seagle CM, Engle CL, Troy Nagle H, Johnson TA, et al. Use of micromachined probes for the recording of cardiac electrograms in isolated heart tissues. Biosens Bioelectron 2004;19:1109–16.
Kovacs GTA. Introduction to the theory, design, and modeling of thin-film microelectrodes for neural interfaces. In: Stenger DA, McKenna T, editors. Enabling Technologies for Cultured Neural Networks. New York: Academic Press; 1994. p. 121–65.

Lee IS, Whang CN, Choi K, Choo MS, Lee YH. Characterization of iridium film as a stimulating neural electrode. Biomaterials 2002;23:2375–80.
Lee K, He J, Clement R, Massia S, Kim B. Biocompatible benzocyclobutene (BCB)-based neural implants with micro-fluidic channel. Biosens Bioelectron 2004a;20:404–7.
Lee K, Singh A, He J, Massia S, Kim B, Raupp G. Polyimide based neural implants with stiffness improvement. Sens Actuatators: B Chem 2004b;102:67–72.
Ludwig KA, Uram JD, Yang J, Martin DC, Kipke DR. Chronic neural recordings using silicon microelectrode arrays electrochemically deposited with a poly(3,4-ethylenedioxythiophene) (PEDOT) film. J Neural Eng 2006;3:59–70.
Manku T, Orchard-Webb JH. Reliability problems of polysilicon/Al contacts due to grain-boundary enhanced thermomigration effects. IEEE Trans Reliab 1995;44:550–5.
Maynard EM, Fernandez E, Normann RA. A technique to prevent dural adhesions to chronically implanted microelectrode arrays. J Neurosci Methods 2000;97:93–101.
Nenadic Z, Burdick JW. Spike detection using the continuous wavelet transform. IEEE Trans Biomed Eng 2005;52:74–87.
Norlin P, Kindlundh M, Mouroux A, Yoshida K, Hofmann UG. A 32-site neural recording probe fabricated by DRIE of SOI substrates. J Micromechan Microeng 2002;12:414–9.
Paik SJ, Park Y, Cho DI. Roughened polysilicon for low impedance microelectrodes in neural probes. J Micromechan Microeng 2003;13:373–9.
Paxinos G, Watson C. The Rat Brain in Stereotaxic Coordinates. Academic Press; 2007.
Polikov VS, Tresco PA, Reichert WM. Response of brain tissue to chronically implanted neural electrodes. J Neurosci Methods 2005;148:1–18.
Richardson RR, Miller JA, Reichert WM. Polyimides as biomaterials: preliminary biocompatibility testing. Biomaterials 1993;14:627–35.
Rousche PJ, Normann RA. Chronic intracortical microstimulation (ICMS) of cat sensory cortex using the Utah intracortical electrode array. IEEE Trans Rehab Eng 1999;7:56–68.
Rousche PJ, Pellinen DS, Pivin Jr DP, Williams JC, Vetter RJ, Kirke DR. Flexible polyimide-based intracortical electrode arrays with bioactive capability. IEEE Trans Biomed Eng 2001;48:361–71.
Schwartz AB, Cui XT, Weber DJ, Moran DW. Brain-controlled interfaces: movement restoration with neural prosthetics. Neuron 2006;52:205–20.
Seymour JP, Kipke DR. Neural probe design for reduced tissue encapsulation in CNS. Biomaterials 2007;28:3594–607.
Shi LH, Luo F, Woodward DJ, Chang JY. Basal ganglia neural responses during behaviorally effective deep brain stimulation of the subthalamic nucleus in rats performing a treadmill locomotion test. Synapse 2006;59:445–57.
Snider RK, Bonds AB. Classification of non-stationary neural signals. J Neurosci Methods 1998;84:155–66.
Subbaroyan J, Martin DC, Kipke DR. A finite-element model of the mechanical effects of implantable microelectrodes in the cerebral cortex. J Neural Eng 2005;2:103–13.
Sugitani M, Yano J, Sugai T, Ooyama H. Somatotopic organization and columnar structure of vibrissae representation in the rat ventrobasal complex. Exp Brain Res 1990;81:346–52.
Suner S, Fellows MR, Vargas-Irwin C, Nakata GK, Donoghue JP. Reliability of signals from a chronically implanted, silicon-based electrode array in non-human primate primary motor cortex. IEEE Trans Neural Syst Rehab Eng 2005;13:524–41.
Szarowski DH, Andersen MD, Retterer S, Spence AJ, Isaacson M, Craighead HG, et al. Brain responses to micro-machined silicon devices. Brain Res Protoc 2003;983:23–35.
Tae Hwan Y, Eun Jung H, Dong Yong S, Se Ik P, Seung Jae O, Sung Cherl J, et al. A micromachined silicon depth probe for multichannel neural recording. IEEE Trans Biomed Eng 2000;47:1082–7.
Townsend G, Peloquin P, Kloosterman F, Hetke JF, Leung LS. Recording and marking with silicon multichannel electrodes. Brain Res Protoc 2002;9:122–9.
Turner JN, Shain W, Szarowski DH, Andersen M, Martins S, Isaacson M, et al. Cerebral astrocyte response to micromachined silicon implants. Exp Neurol 1999;156:33–49.
Vetter RJ, Williams JC, Hetke JF, Nunamaker EA, Kipke DR. Chronic neural recording using silicon-substrate microelectrode arrays implanted in cerebral cortex. IEEE Trans Biomed Eng 2004;51:896–904.
Xu C, Lemon W, Liu C. Design and fabrication of a high-density metal microelectrode array for neural recording. Sens Actuators A: Phys 2002;96:78–85.